Korean J. Chem. Eng., 32(9), 1918-1923 (2015)
DOI: 10.1007/s11814-014-0392-9

pISSN: 0256-1115
eISSN: 1975-7220

New α-$Zn_2V_2O_7$/carbon nanotube nanocomposite for supercapacitors

Nulu Venugopal and Woo-Sik Kim†

Department of Chemical Engineering, College of Engineering, Kyung Hee University,
1 Seochon, Giheung-gu, Yongin-si, Gyeonggi-do 446-701, Korea
(*Received 8 July 2014 • accepted 28 December 2014*)

Abstract−This study synthesized α-$Zn_2V_2O_7$ nanopowders using a hydrothermal approach followed by annealing treatment. The resulting powders were then mixed with multi-walled carbon nanotubes and electrochemically characterized as new nanocomposite electrodes for supercapacitors. The structure and surface morphology of the powders were characterized by X-ray diffraction, transmission electron microscopy, and scanning electron microscopy. Plus, the capacitive behavior of the composite electrodes was evaluated by cyclic voltammetry and galvanostatic charge-discharge cycles in different molar aqueous KCl solutions. The α-$Zn_2V_2O_7$/multi-walled carbon nanotube composite electrodes were prepared using three different ratios and screened for their use in supercapacitors. As a result, the α-$Zn_2V_2O_7$/multi-walled carbon nanotube composite electrode with a 1 : 2 ratio was identified as the best electrode with a specific capacitance value of 44.8 F g^{-1} in 0.5 M KCl. Notwithstanding, all the tested composite electrodes demonstrated an excellent cycle stability and showed a less than 4% change in their specific capacitance values when compared to the initial values.

Keywords: Nano Zinc Pyrovanadate, Carbon Nanotubes, Composite Electrode, Aqueous Electrolyte

INTRODUCTION

Supercapacitors can store a greater amount of energy than conventional capacitors and deliver more power than batteries, making them an emerging energy storage alternative. Furthermore, supercapacitors, also known as electrochemical capacitors or ultracapacitors, fill the gap between batteries and conventional capacitors [1]. Based on their energy storage mechanism, supercapacitors can be classified as both an electrical double-layer capacitor (EDLC) and a pseudo-capacitor. The capacitance of the former comes from the charge accumulation at the electrode/electrolyte interface, thereby strongly depending on the surface area of the electrode accessible to the electrolyte. Meanwhile, the capacitance of the latter is due to the reversible faradic reaction of the electro-active species of the electrode, such as surface functional groups and transition metal oxides. Thus, the electrode is clearly the key for the development of supercapacitors [2].

One approach to enhancing the specific capacitance is to add a pseudo-capacitor component to EDLC electrodes [3-5]. Considerable effort has already been devoted to the development and characterization of new electrode materials with a lower cost and improved performance. While carbon electrode materials have a low cost, their capacitance is limited. Therefore, cheaper candidates with good capacitive characteristics have been attracting significant attention. Various studies have found that new composite binary, mixed metal oxides, like microporous nickel-manganese oxide, cobalt-manganese oxide, annealed Mn-Fe binary oxides, Ru-Co mixed oxides on the surface of single-walled carbon nanotubes, and ruthenates based on $SrRuO_3$ perovskite, exhibit pseudo capacitance behavior, while $LiNi_{0.8}Co_{0.2}O_2$/MWCNT composite electrodes have good capacitive and energy characteristics [6-10]. Zinc Oxide (ZnO), due to its promising electrical and optical properties, has also been evaluated for application in supercapacitors as a composite electrode in combination with carbon-aerogel; CNT composite film and with carbon in a basic gel polymer solid state electrolyte; and ZnO/C in an aqueous KNO_3 solution [11-13]. Most recent research efforts have been focused on using more environmentally-friendly electrolytes instead of concentrated acid or alkali. Moreover, vanadium pentoxide has versatile redox-dependent properties due to the multiple valence states of vanadium, providing a good capacitive performance in neutral solutions [14]. It has already been established that mixed 3d-transition metal oxides are more active than simple oxides [15-20]. α-$Zn_2V_2O_7$ is isostructural with β-$Cu_2V_2O_7$ and was first reported by Gopal and Calvo [21]. Plus, $(Zn_{2x}Cu_x)V_2O_7$ solid-solutions have been synthesized by heating to 1,000 °C, followed by cooling to 750 °C and quenching [22].

Accordingly, this study synthesized pyrovanadate α-$Zn_2V_2O_7$ nanoparticles using a hydrothermal method followed by calcination and then applied this new material as a composite electrode in combination with multi-walled carbon nanotubes for use in supercapacitorss.

EXPERIMENTAL

1. Chemicals

All the reagents were of analytical-reagent grade and used as received. The water used in all the experiments was doubly distilled. High purity N_2 was used to remove the oxygen from the solution. All the experiments were carried out at room temperature (20±5 °C).

†To whom correspondence should be addressed.
E-mail: wskim@khu.ac.kr
‡This article is dedicated to Prof. Hwayong Kim on the occasion of his retirement from Seoul National Univerisity.

2. Synthesis of Zinc Pyro Vanadate, α-$Zn_2V_2O_7$

In brief, the precursor solution with a mole ratio of V/Zn=1 was prepared by mixing the starting materials NH_4VO_3 (0.05 M) and $Zn(NO_3)_2{\cdot}6H_2O$ (0.05 M) in 400 ml of water, followed by the addition of urea (0.1 M) and transfer into an autoclave. Next, the solution temperature was increased to 200 °C during 1 hr (ramp time) and the reaction then maintained at this temperature for 4 hrs (soak time) with an in-situ pressure of around 18-20 kg cm^{-2}. Thereafter, the solution was cooled to room temperature during 2 hrs, at which point the product was filtered, washed with water and acetone, and dried at 110 °C in a hot air oven. While the initial pH of the experimental solution was acidic (pH~4), the final pH was alkaline (pH~7.8). Finally, the powder was calcined at 500 °C for 2 hrs.

3. Material Characterization

The powder XRD data for the samples was obtained using a Siemens D 5000 X-ray diffractometer with Bragg-Brentano geometry and Cu Kα radiation (λ=1.5418 Å). The samples were scanned for their 2θ values within a range of 2 to 80°. The transmission electron microscope (TEM) images were obtained using a PHILIPS made Tecnai-12 FEI instrument operated at an accelerating voltage of 100 kV. The SEM analysis was conducted using a scanning electron microscope, Leo 440 (Germany), equipped with an Econ 4 detector (EDAX, USA).

4. Electrode Preparation and Electrochemical Measurements

The α-$Zn_2V_2O_7$ powder was mixed with the multiwalled carbon nanotubes (in-short CNT, supplied from ILJIN Nanotech Company Ltd.) in a ratio of ZVC11 (1 : 1), ZVC12 (1 : 2), and ZVC21 (2 : 1) using ultrasonic agitation in ethanol for 10 min, followed by drying and physical mixing. The electrodes for the electrochemical capacitors were prepared by mixing the prepared powders (70 wt%) with 25 wt% carbon black as the conductive agent and 5 wt% of the PTFE binder to make the total electrode mass. A small amount of ethanol was added to the composite for coating a stainless steel (SS) mesh (0.5 cm×0.5 cm) that was used as the current collector. The resulting electrodes were pressed at a pressure of 10 MPa for 1 min and subsequently dried at 373 K for 12 h. All the electrochemical measurements were taken based on a three-electrode arrangement using a PGSTAT 30 Auto lab system (Ecochemie, Utrecht, the Netherlands) connected to a PC with Eco-Chemie GPES software. The GPES software was used for all the electrochemical data analyses. The reference electrode was Ag/AgCl (3M KCl), while the counter electrode was a platinum foil supplied with the instrument. The electrodes were tested in 0.1 M, 0.5 M, and 1 M KCl aqueous electrolyte solutions.

RESULTS AND DISCUSSION

1. Formation of α-$Zn_2V_2O_7$

The XRD patterns for the as-prepared and calcined samples of zinc pyrovanadate prepared by urea hydrolysis under hydrothermal conditions are given in Figs. 1(a) and (b). The XRD peaks for the as-prepared sample were indexed to both $Zn_3(OH)_2V_2O_7{\cdot}2H_2O$ (JCPDS 50-0570) and VO_2 peaks; $Zn_3(OH)_2V_2O_7{\cdot}2H_2O$ was present as the major phase and the peaks were sharper and broader, indicating a good crystallinity (see Fig. 1(a)). A blackish white precipitate was obtained after 4 hrs of continuous stirring under the hydrothermal conditions at a 20 kg cm^{-2} pressure, which then turned into an orange tinted white α-$Zn_2V_2O_7$ powder after calcination at 500 °C for 2 hrs. The X-ray diffractogram of the blackish white precipitate revealed a crystalline phase, the diffraction peaks for which agreed well with a previously published X-ray diffractogram of zinc pyrovanadate with a small amount of VO_2 as a minor phase [23].

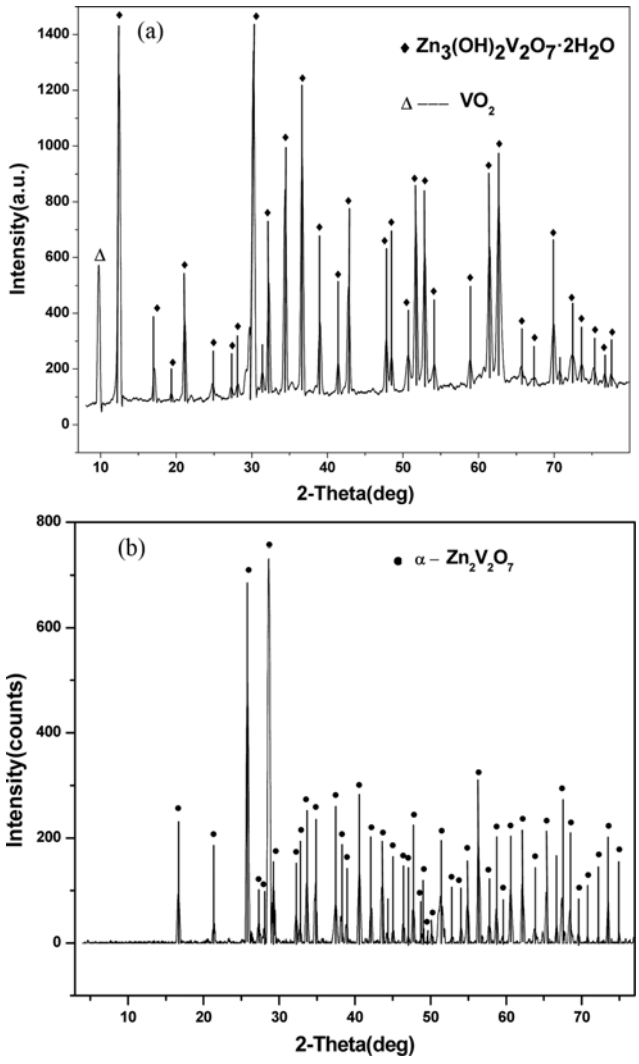

Fig. 1. X-Ray diffraction patterns of the (a) as prepared $Zn_3(OH)_2V_2O_7{\cdot}2H_2O$ (b) $Zn_3(OH)_2V_2O_7{\cdot}2H_2O$ calcined at 500 °C for 2 hrs in presence of air, α-$Zn_2V_2O_7$ (monoclinic structure).

Fig. 1(b) shows the evolution of the X-ray diffraction pattern for the pure α-$Zn_2V_2O_7$ phase obtained using thermal decomposition of the as-prepared sample at 500 °C for 2 hrs., which was found to be monoclinic with space group *C*2/c and lattice parameters of a= 7.429 Å, b=8.340 Å, and c=10.098 Å [24]. In the calcined sample, as expected, while the $Zn_3(OH)_2V_2O_7{\cdot}2H_2O$ phase disappeared, α-$Zn_2V_2O_7$ (monoclinic structure, JCPDS 70-1532) [24] developed as the single phase, plus the peaks had a higher intensity and were sharper than those for the as-prepared sample, indicating a good crystallinity on a nano-scale dimension. The scanning electron micrograph of α-$Zn_2V_2O_7$ in Fig. 2(a) shows the morphology on a micro-scale dimension, in which case the particles appear as clus-

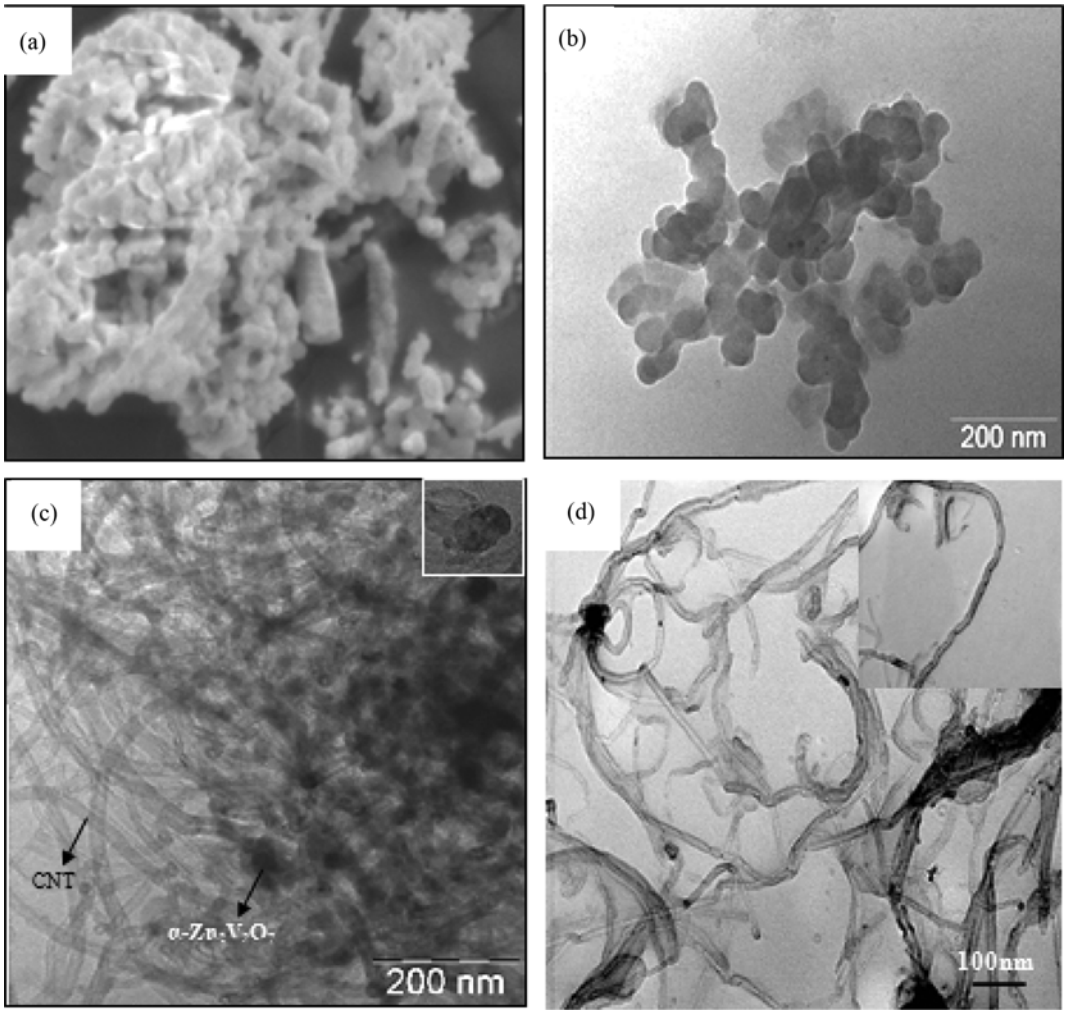

Fig. 2. (a) SEM and (b) TEM images of α-$Zn_2V_2O_7$ nanoparticles, (c) TEM image of composite ZVC12 (1 : 2), inset shows the close view of the specific nanoparticle attached to the carbon nanotube, (d) TEM image of multiwalled carbon nanotubes.

ters due to agglomeration; however, the distribution of the nanoparticles (50-60 nm) can be seen more clearly in the TEM image in Fig. 2(b), where the average particle size is between 50-55 nm. Meanwhile, Fig. 2(c) shows the distribution of the carbon nanotubes, where the dark surface of the image shows the presence of α-$Zn_2V_2O_7$ nanoparticles dispersed on the outer surface of the carbon nanotubes, plus Fig. 2(d) shows a TEM image of the carbon nanotubes (Nanotech Int. Ltd) with an average carbon nanotube width of around 10-12 nm.

2. Electrochemical Studies

The cyclic voltammetry (CV) response is a valuable tool to determine the performance of an electrode for a supercapacitor. Fig. 3(a) shows the voltammetric responses of the pure CNT and composite ZVC11 (1 : 1) electrode in a 0.1M KCl solution at a sweeping rate of 0.1 Vs^{-1}. The specific capacitance can be calculated using the following equation:

$$\text{Specific capacitance (CV)}\ (F\ g^{-1}) = Q(c)/[\Delta E(V)\ m(g)] \quad (1)$$

Here, Q is the charge in coulombs, ΔE the potential difference in volts, and m the active material mass in grams. Table 1 shows the specific capacitance calculated for the anodic and cathodic scans in the case of the initial and 100th scan.

In an earlier study by the present authors, the specific capacitance values for CNT obtained in dilute KCl solutions were lower than the present values, yet the shape of the CV was that of a perfect double layer capacitor [25]. Thus, the higher values in the present study can be attributed to the electrode preparation method. In the previous study, the CNT was immobilized mechanically on a graphite electrode, hence the difference in the active material construction of the electrode evidently produced the observed difference in the specific capacitance. The present voltammograms generally stabilized after the first cycle. As expected and revealed by the capacitance values obtained for the first and 100th cycles, the value for the composite ZVC11 was three times higher than that for the pure CNT; this difference was due to the pseudocapacitive contribution of the metal oxides against the only double layer capacitance of the CNT electrode. Fig. 3(b) shows the CV responses for the composite ZVC11 in 0.5 M, 1 M, and 0.1 M KCl solutions, where the specific capacitances increase when increasing the concentration of KCl in the electrolyte solution, yet decrease with cycling. While

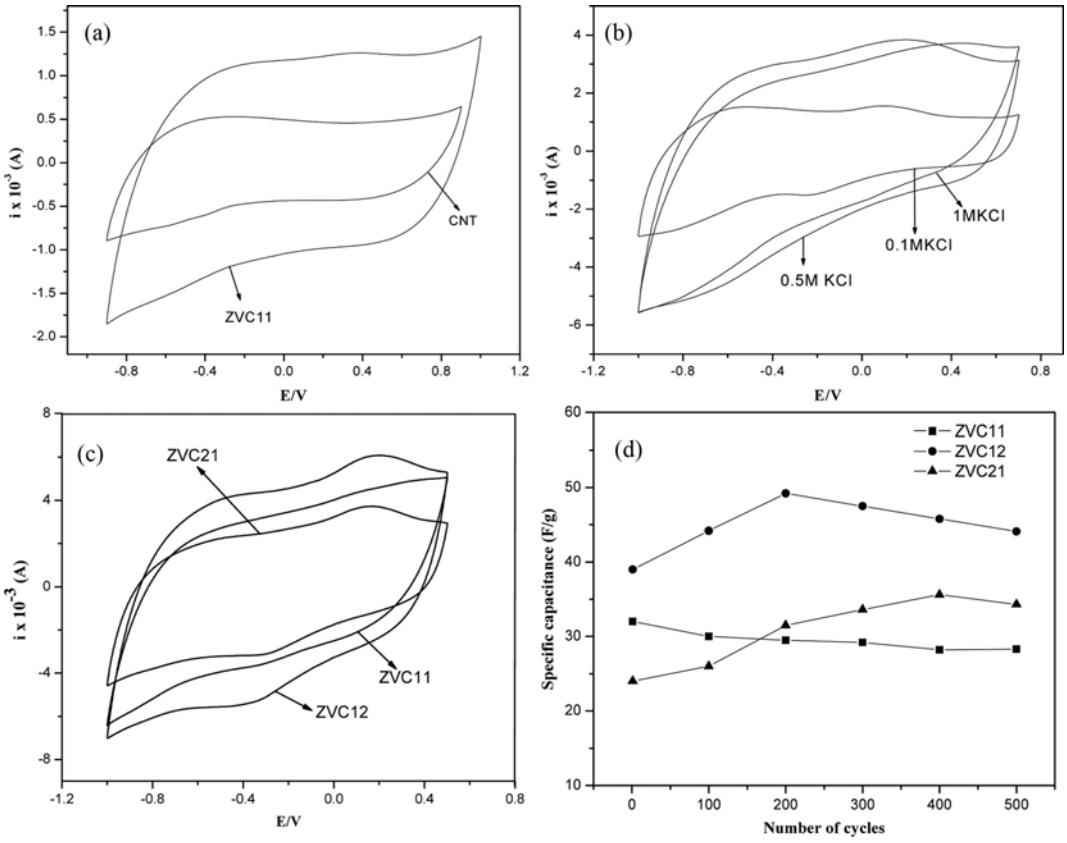

Fig. 3. Cyclic voltammograms for 100th scan of (a) pure CNT and composite ZVC11 (1 : 1) electrode in 0.1 M KCl solution, (b) in 0.1 M, 0.5 M and 1 M KCl solutions, (c) 100th scan of ZVC11, ZVC12 and ZVC21 electrodes in 0.5 M KCl solution, (d) comparison of the CV profiles and cycling performance of the different composite electrolytes; all the electrodes are tested at a constant scan rate of 0.1 V s^{-1}.

Table 1. Specific capacitance values of bare CNT and ZVC11 (1 : 1) calculated from the cyclic voltammograms; scan rate, 100 mVs^{-1}; electrolyte 0.1 M KCl

Electrode	Specific capacitance (Fg^{-1})			
	Anodic scan		Cathodic scan	
	1	100	1	100
CNT	4.5	4.6	4.2	4.1
ZVC11	16	14.1	15.1	15.5

Table 2. Specific capacitance values calculated from the cyclic voltammograms of ZVC11 (1 : 1) in 0.1 M, 0.5 M, 1 M KCl; scan rate, 100 mVs^{-1}

Electrolyte solution	Specific capacitance (Fg^{-1})	
	Cycle no.	
	1st	100th
0.1 M KCl	16	14.1
0.5 M KCl	31	35
1 M KCl	34	26

the specific capacitance was doubled when increasing the KCl concentration in the electrolyte solution from 0.1 M to 0.5 M, a further concentration increase to 1.0 M KCl did not increase the capacitance, suggesting the saturation of the electrode surface, and resulted in a decline of the specific capacitance (see Table 2). In fact, the 1 M KCl seemed to deteriorate the electrode with continuous cycling.

Thus, 0.5 M KCl was clearly the ideal electrolyte concentration to obtain a better capacitance. As the non-faradic double layer capacitance increases due to the ion alignment at the electrode/electrolyte interface, this increases the population of charged ions in the proximity of the electrode surface, thereby producing a change in resonance with an equally charged electrode surface, which explains the capacitance of 32 Fg^{-1} observed with 0.5 M KCl in contrast to 16 Fg^{-1} observed with 0.1KCl. However, the decreased capacitance of the 100th cycle for both the dilute and strong concentrations of KCl reflects the concentration from the faradic charge transfer of the composite electrode, which may be irreversible.

Fig. 3(c) compares the CV profiles of the α-$Zn_2V_2O_7$ - CNT composite electrodes with different ratios, measured at a scan rate of 100 mVs^{-1}. The different shapes of the CV profiles according to the composite materials were attributed to the different capacitance values. When using a 0.5 M KCl solution, the area of the active electrode material was increased in the CV scan for α-$Zn_2V_2O_7$ - CNT (1 : 2) when compared to the CV scans for α-$Zn_2V_2O_7$ - CNT (1 : 1) and α-$Zn_2V_2O_7$ - CNT (2 : 1). Thus, when increasing the CNT content in the composite electrode with α-$Zn_2V_2O_7$ nanoparticles (ZVC12),

Table 3. Specific capacitance values calculated from the cyclic voltammograms of α-$Zn_2V_2O_7$: CNT in the ratios 1 : 1 (ZVC11), 1 : 2 (ZVC12), 2 : 1 (ZVC21) in 0.5 M KCl; scan rate, 100 mVs^{-1}

Electrode	Specific capacitance (Fg^{-1})			
	Anodic scan		Cathodic scan	
	1	100	1	100
ZVC11	31	35	30.8	33.52
ZVC12	39	44.8	35.4	46.8
ZVC21	24	26	19.5	27.60

this increased the surface area and porosity of the electrode material, along with the pseudocapacitive behavior of the α-$Zn_2V_2O_7$ nanoparticles. The specific capacitance values are presented in Table 3, while the cycling performances of all three composite electrodes are shown in Fig. 3(d). For the ZVC12 composite electrode, the specific capacitance value clearly increased from the first cycle to the 200th cycle, although after 200 cycles, the ZVC12 composite capacitor showed an average capacitance decrease of 3.4%. Meanwhile, the specific capacitance value increased 2% from the first cycle to the 400th cycle for the ZVC21 composite electrode, and decreased 3.4% from the first cycle to the 500th cycle for the ZVC11 composite electrode. Notwithstanding, the ZVC12 composite produced better specific capacitance values than ZVC11 and ZVC21, even at the 500th cycle. Interestingly, parallel specific capacitance values were observed for the ZVC11 and ZVC21 composites, even though the latter had a higher mass of mixed metal oxide than the former. This was attributed to the redox properties of α-$Zn_2V_2O_7$ in the composite materials, as well as the effect of the particle size on the utilization of the pseudo active species.

The supercapacitive characteristics were also measured using a constant current charge-discharge cycling test, which provides a better quantitative insight into the supercapacitive nature of an electrode material and where the ideal capacitive nature of an active

Table 4. Specific capacitance values calculated from the galvanostatic charge-discharge curves in 0.5 M KCl solution at a constant current density of 0.1 Ag^{-1}

Cycle no.	Specific capacitance (Fg^{-1})		
	ZVC11	ZVC12	ZVC21
1	30.12	38.32	31.25
100	18.21	29.11	16.44
500	10.71	20.83	13.28

material is indicated by a straight line charge-discharge curve. Thus, the α-$Zn_2V_2O_7$: CNT composite electrodes with ratios of 1 : 1, 1 : 2, and 2 : 1 were subjected to charge-discharge studies using double potential step chrono potentiograms. At a constant current density of 0.1 Ag^{-1} in 0.5 M KCl, the samples were subjected to 500 cycles and the results tabulated (see Table 4). Figs. 4(a) and (b) show the typical plots obtained for ZVC11, ZVC12, and ZVC21 at the 100th cycle and 500th cycle, respectively, while Fig. 4(c) shows the variation in the capacitance stability according to the cycle number. The curves were all essentially straight lines, a trademark of capacitive charge-discharge behavior. Plus, the specific capacitance values decreased gradually from the initial cycle, although the highest value was for ZVC12 (38.32 Fg^{-1}). A sudden potential drop was noted for all the composite electrodes at the very beginning of the constant current discharge, which is usually observed for EDLCs and called the IR drop. Liu et al. previously reported that this potential drop is due to the resistance of the electrolytes, contact resistance between the carbon and the current collector, and inner resistance of the ion migration in the carbon micropores [26].

One explanation for the significant decrease in resistance at the 500th cycle for all the composite electrodes is that after the electrodes were soaked in the electrolyte, the presence of CNTs not only favored ionic diffusion but also possibly reduced the connection resistance between the CNT- α-$Zn_2V_2O_7$ composite and the current collector. The variations in the discharge capacitance according to the cycle number also showed a lower decrease in capacitance after 250 cycles.

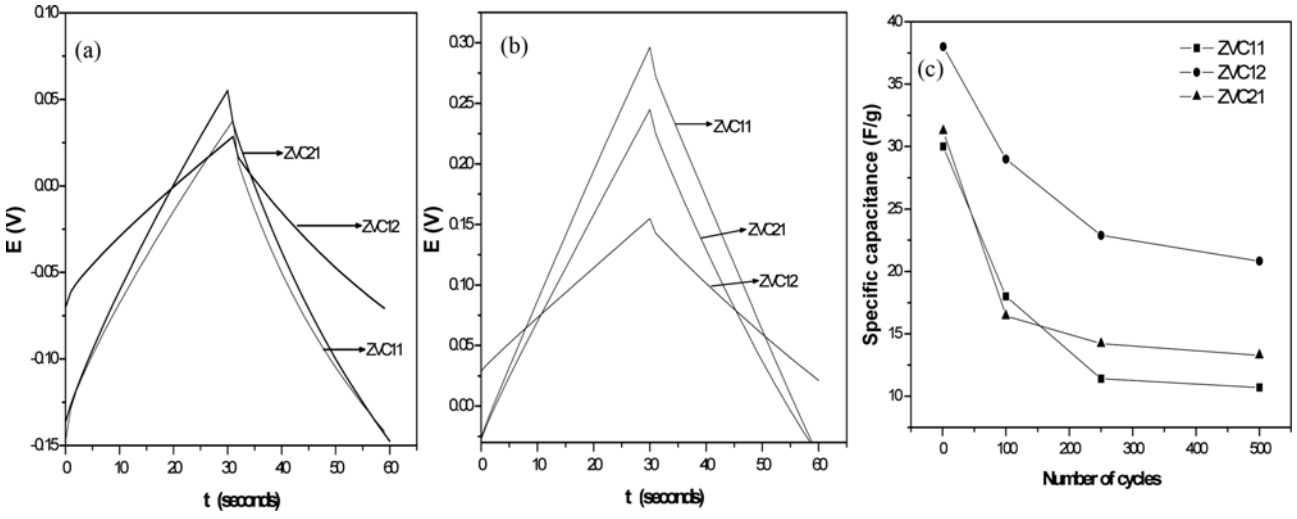

Fig. 4. Galvanostatic charge–discharge plots of nanocomposite electrodes, (a) ZVC11, ZVC12 and ZVC21 respectively recorded for 100th cycle, (b) 500th cycle, (c) cycle-life of the electrodes at a constant current density of 0.1 Ag^{-1}.

Overall, the capacitance values showed that the capacitance of ZVC12 (38.32 Fg^{-1}) was higher than that of ZVC11 and ZVC21. Specifically, at the 500th cycle, ZVC12 showed a higher capacitance than ZVC11 and ZVC21, indicating that the higher percentage of CNT combined with the pseudo capacitance of α-$Zn_2V_2O_7$ produced a higher number of pores (range 5-15 nm) in the composite electrode, which in turn led to the additional specific capacitance of the nanocomposite electrode in the aqueous neutral electrolyte.

CONCLUSIONS

We synthesized nano particles of α-$Zn_2V_2O_7$ based on thermal treatment of the product obtained from a urea-assisted hydrothermal method, and then investigated the application of the new material in a supercapacitor with an aqueous electrolyte when using a composite electrode material including CNT at ratios of 1 : 1, 1 : 2, and 2 : 1. The $Zn_2V_2O_7$/CNT composites exhibited good capacitor properties and different capacitive behaviors depending on the CNT content, and among these electrodes the electrode with 1 : 1 ratio showed superior performance due to the better dispersion of metal oxide nanoparticles on CNT networks, which resulted in maximum amount of metal oxide surface exposed to the electrolyte during analysis. In cyclic voltammetry studies, all the composite electrodes showed a good cycling stability up to 500 cycles with a less than 4% loss of the specific capacitance. The best specific capacitance value was up to 44.8 Fg^{-1} when using the α-$Zn_2V_2O_7$/CNT (1 : 2) composite electrode in a 0.5 M KCl solution.

ACKNOWLEDGEMENT

This work was financially supported by the Kyung Hee University Research Program (2013).

REFERENCES

1. A. Burke, *J. Power Sources*, **91**, 37 (2000).
2. B. E. Conway, *Electrochemical supercapacitors*: *Scientific fundamentals and technological applications*, Kluwer Academic/Plenum Publisher, New York (1999).
3. B. J. Lee, S. R. Sivakkumar, J. M. Ko, J. H. Kim, S. M. Jo and D. Y. Kim, *J. Power Sources*, **168**, 546 (2007).
4. Y. Shan and L. Gao, *Mater. Chem. Phys.*, **103**, 206 (2007).
5. G. Arabale, D. Wagh, M. Kulkarni, I. S. Mulla, S. P. Vernekar, K. Vijayamohanan and A. M. Rao, *Chem. Phys. Lett.*, **376**, 207 (2003).
6. K. Rajendra Prasad and N. Miura, *Electrochem. Commun.*, **6**, 1004 (2004).
7. M. T. Lee, J. K. Chang, Y. T. Hsieh and W. T. Tsai, *J. Power Sources*, **185**, 1550 (2008).
8. B. C. Kim, G. G. Wallace, Y. I. Yoon, J. M. Ko and Ch. O. Too, *Synthetic Met.*, **159**, 1389 (2009).
9. M. W. Mehrens, J. Schenk, P. M. Wilde, E. Abdelmula, P. Axmann and J. Garche, *J. Power Sources*, **105**, 182 (2002).
10. G. Wang, M. Qu, Z. Yu and R. Yuan, Mater. *Chem. Phys.*, **105**, 169 (2007).
11. D. Kalpana, K. S. Omkumar, S. Suresh Kumar and N. G. Renganathan, *Electrochim. Acta*, **52**, 1309 (2006).
12. Y. Zhang, X. Sun, L. Pan, H. Li, Z. Sun, C. Sun and B. K. Tay, *J. Alloy. Compd.*, **480**, 17 (2009).
13. M. Jayalakshmi, M. Palaniappa and K. Balasubramanian, *Int. J. Electrochem. Sci.*, **3**, 96 (2008).
14. H. Y. Lee and J. B. Goodenough, *J. Solid State Chem.*, **148**, 81 (1999).
15. A. Naydenov and D. Mehandjiev, *Compt. Rend. Acad. Bulg. Sci.*, **46**, 49 (1993).
16. G. M. Bliznakov and D. R. Mehandjiev, *Kinet. Catal.*, **28**, 116 (1987).
17. A. T. Baricevic, B. Grbic, D. Jovanovic, S. Angelov, D. Mehandjiev, C. Marinova and P. K. Stefanov, *Appl. Catal.*, **47**, 145 (1989).
18. D. R. Mehandjiev and I. P. Dimitrova, *Compt. Rend. Acad. Bulg. Sci.*, **42**, 71 (1989).
19. S. Angelov, D. R. Mehandjiev, B. Piperov, V. Zarkov, A. T. Baricevic, D. Jovanovic and Z. Jovanovic, *Appl. Catal.*, **16**, 431 (1985).
20. E. Dyakova, A. T. Baricevic, D. Mehandjiev, E. Zhecheva and B. Grbic, *React., Kinet. Catal. Lett.*, **43**, 521 (1991).
21. R. Gopal and C. Calvo, *Can. J. Chem.*, **51**, 1004 (1973).
22. M. Schindler and F. C. Hawthorne, *J. Solid State Chem.*, **146**, 271 (1999).
23. P. Y. Zavalij, F. Zhang and M. S. Whittingham, *Acta Crystallogr., Sect. C*, **53**, 1738 (1997).
24. S. Daniel Abraham, S. Theodore David, R. Biju Bennie, C. Joel, M. Seethamahalakshmi and T. Adinavven, *Chem. Sci. Transactions*, **3**(4), 1488 (2014).
25. M. Jayalakshmi, M. Mohan Rao, N. Venugopal and K. B. Kim, *J. Power Sources*, **166**, 578 (2007).
26. X. Liu and T. Osaka, *J. Electrochem. Soc.*, **144**, 3066 (1997).